PREPRINT
IN-02
AVAIL/CASI
@ WAIVED

AIAA 2000-0410

Sweep and Compressibility Effects on Active Separation Control at High Reynolds Numbers

Avi Seifert and LaTunia G. Pack

NASA Langley Research Center

Hampton, VA

38th AIAA Aerospace Sciences Meeting and Exhibit
January 10-13, 2000/ Reno, NV

Sweep and Compressibility Effects on Active Separation Control at High Reynolds Numbers

Avi Seifert[*] and LaTunia G. Pack[†]
NASA Langley Research Center, Hampton, VA

Abstract

This paper explores the effects of compressibility, sweep and excitation location on active separation control at high Reynolds numbers. The model, which was tested in a cryogenic pressurized wind tunnel, simulates the upper surface of a 20% thick Glauert-Goldschmied type airfoil at zero angle of attack. The flow is fully turbulent since the tunnel sidewall boundary layer flows over the model. Without control, the flow separates at the highly convex area and a large turbulent separation bubble is formed. Periodic excitation is applied to gradually eliminate the separation bubble. Two alternative blowing slot locations as well as the effect of compressibility, sweep and steady suction or blowing were studied. During the test the Reynolds numbers ranged from 2 to 40 million and Mach numbers ranged from 0.2 to 0.7. Sweep angles were 0 and 30 deg.

It was found that excitation must be introduced slightly upstream of the separation region regardless of the sweep angle at low Mach number. Introduction of excitation upstream of the shock wave is more effective than at its foot. Compressibility reduces the ability of steady mass transfer and periodic excitation to control the separation bubble but excitation has an effect on the integral parameters, which is similar to that observed in low Mach numbers. The conventional swept flow scaling is valid for fully and even partially attached flow, but different scaling is required for the separated 3D flow. The effectiveness of the active control is not reduced by sweep. Detailed flow field dynamics are described in the accompanying paper.

Nomenclature

c_μ steady blowing momentum coefficient, $\equiv J/cq$

$\langle c_\mu \rangle$ oscillatory blowing momentum coefficient, $\equiv <J'>/cq$

C_μ combined blowing momentum coefficient, $\equiv \left(c_\mu ; <c_\mu > \right)$

c model chord

C_n normal force coefficient

C_{dp} pressure drag coefficient

C_m moment coefficient

C_p wall pressure coefficient, $\equiv (P - P_S)/q$

$C_{p,min}$ minimum pressure coefficient

$\Delta C_{p,rec}$ pressure rise from $C_{p,min}$ to $c_{p,S}$

f oscillation frequency [Hz]

F^+ reduced frequency, $\equiv (f \, x_{sp})/U_\infty$

h slot height or width

J momentum at slot exit, $\equiv \rho h U_j^2$

M Mach number

P pressure

q free stream dynamic pressure, $\equiv 1/2\rho U_\infty^2$

R_c chord Reynolds number, $\equiv U_\infty c/v$

T temperature

U, u average and fluctuating streamwise velocity

w fluctuating spanwise velocity

x/c normalized streamwise location

X_{sp} distance from baseline separation to reattachment

z spanwise location

Λ sweep angle [deg]

v kinematic viscosity

ρ density

Abbreviations

LE   leading edge

TE   trailing edge

< >   phase locked values

Subscripts

b   baseline flow conditions

c   cavity

crit   sonic conditions

d   de-rectified hot-wire data

j   conditions at blowing slot

N   Normalized according to text

R   reattachment

S   separation

∞ free-stream conditions

2D   two-dimensional

3D   three-dimensional

Superscripts

′   root mean square of fluctuating value

* Senior lecturer, Dep. of Fluid Mechanics & Heat transfer, Faculty of Engineering, Tel-Aviv University, Ramat Aviv 69978, Israel, member AIAA.

† Research Engineer, Flow Physics and Control Branch, member of AIAA.

1. Introduction

Boundary layer control (BLC) research dates back to the turn of the 20th century (e.g. Prandtl, in Ref. 1). However, low efficiency, complexity and maintenance difficulties prevented the utilization of laboratory proven BLC techniques, such as blowing or suction. Forced oscillations superposed on a mean flow that is on the verge of separating were previously found to be very effective in delaying turbulent boundary layer separation[2]. Experiments performed on various existing airfoils at low and high Reynolds numbers[3-5], demonstrated that even if the flow is not fully attached, the lift could be significantly enhanced by the introduction of periodic excitation into the separated shear-layer. This is achieved by exciting the flow at frequencies that generate 2-4 spanwise coherent vortices over the length of the separated region (i.e. $F^+ \approx 1$). The addition of periodic excitation into a separating turbulent boundary layer increases the momentum transfer across the shear-layer, enhancing its resistance to separation under adverse pressure gradient. The technique was also demonstrated at high Reynolds number compressible speeds[6]. Though demonstrated experimentally, active separation control using periodic excitation is still a challenge for numerical simulation, while design tools are not available.

The appropriate use of active BLC should enable simplified, cheaper, more efficient and reliable systems, while maintaining performance. A multi-disciplinary design optimization process should allow simplified high-lift systems, thicker airfoils that will allow lighter structures and greater internal volume, shorter aft bodies, size reduction and even elimination of conventional control surfaces. Existing design tools are capable of reproducing steady flows, including steady mass transfer. However, the inclusion of unsteady BLC effects into CFD tools has not been performed. The development of a proper CFD design tool is dependent on the availability of a comprehensive database at relevant conditions (i.e. flight Reynolds numbers), to allow its validation.

The present experiment is aimed at improving our understanding of controlling separated flows at flight Reynolds numbers and providing a comprehensive database for validation of unsteady CFD design tools. Specifically we are exploring the effects of compressibility, sweep and location for introduction of the control input. A previous publication[8] presented some of the experimental results for incompressible 2D flow over the same model.

Flow separation at compressible speeds typically occurs downstream of a shock-wave/boundary-layer interaction. The pressure jump across the shock either causes immediate separation or thickens the boundary layer and reduces its momentum such that it separates further downstream. Once the flow separates downstream of the shock, the unsteady separation and subsequent reattachment (if it occurs) induce unsteadiness in both the shock position and strength. This phenomenon is known as buffeting. The low frequency oscillations can cause structural damage, if coupled with the resonance frequencies of the structure. Active control at compressible speeds was demonstrated[6] on a NACA 0015 airfoil. The introduction of periodic excitation upstream of the shock wave improved the performance of the airfoil and reduced the unsteadiness in its wake. The present experiment is intended to supplement the airfoil experiment by providing additional flexibility in the control parameters and more detailed measurements of the mean and fluctuating wall pressures.

Sweep and compressibility are associated in the sense that sweep was initially introduced in order to reduce the effective wing thickness ratio and therefore delay the appearance of shock waves to higher free stream Mach numbers. The importance of separation control over 3D configurations stems from the need to optimize high lift systems of swept wing airplanes as well as other 3D flows. While 2D flow is relatively easy to establish and analyze, quasi "2D" swept flow or "infinitely swept" flow is extremely complicated to duplicate and essentially impossible in the presence of separation. Presently we study the effects of active separation control by rotating the model to a mild sweep of 30 deg and comparing the results to those obtained in the absence of sweep.

Section 2 of this paper provides a brief description of the experimental set-up. Section 3 presents the experimental results, initially of the baseline flow and thereafter those of the controlled flow.

2. Description of the Experiment

2.1 Overview

The set-up of the experiment was described in detail in a previous publication[8]. Only vital details will be provided here.

2.2 The "Hump" model

The model simulates the upper surface of a 20% thick, Glauert- Goldschmied type airfoil. It is installed on the right side tunnel turntable. The reference chord is 200 mm. The original location of the airfoil leading edge is defined as the reference leading edge (Fig. 1). This area was faired smoothly from x/c=-0.05 to 0.05 in order to eliminate slope discontinuity. Two alternative excitation slot locations are available: x/c=0.59 and 0.64. The position of the upstream slot was selected such that it would be upstream of the expected position of a shock wave. The slots were about 0.25% chord wide (0.50±0.10 mm), and allowed an almost tangential downstream introduction of momentum (Fig. 1). The floor and ceiling boundary layers did not affect the spanwise uniformity of the flow over the model that is installed on the sidewall, due to the use of a pair of end

plates (vertical thick lines on Figs. 2 and 3). The gap between the end plates and the tunnel walls was 12.7 mm, which was deemed sufficient, based on the available wind tunnel boundary layer data[7]. Data acquired during this experiment[8] verifies that this gap was sufficient. The tunnel cross-sectional blockage due to the model and end plates is 0.0836. The model allows testing at 0-deg and 30-deg sweep. The swept configuration was achieved by removing certain parts of the model, rotating the turntable on which the model is installed by 30 deg and placing alternative parts of the model and an alternative set of end plates (Fig. 3). The distribution of the pressure taps is also shown in Figs. 2 and 3. The streamwise row contains 34 taps, aligned at about 20 deg with the free stream direction that is also used for the 30-deg swept configuration. Three spanwise rows, of nine pressure taps each, are located at x/c=0, 0.49 and 0.95. The pressure taps are spaced every 25.4 mm (0.127c) and cover half the chord length on each side of the centerline. The swept configuration contains two additional taps on the forward upstream end (Fig. 3). The internal diameter of all pressure tap orifices is 0.254 mm. The model is also instrumented with 12 unsteady pressure transducers (indicated by x symbols on Fig. 2). The transducers are installed under the model surface, inside small volume cavities. The cavities are connected to the surface of the model by tiny orifices, 0.254 mm in diameter. The effect of this installation on the frequency response of the unsteady pressure transducers is complex. It was studied using a comprehensive bench-top calibration and occasional in-situ testing by a Piezo-electric actuator. In addition, one transducer was flush mounted near the trailing edge of the turntable next to a recessed pressure transducer and their readings are compared. The full scale of the unsteady pressure transducers is 10 psid. They are referenced to the static wall pressures immediately next to the orifice locations or to the wind tunnel plenum pressure in order to maintain optimal resolution even at static pressures that exceed the transducer's range. One unsteady pressure transducer is installed inside the model cavity, midway between the end plates and about 30-mm from the slot exit. It is used to monitor the cavity pressure oscillations in the wind tunnel, and to correlate the wind tunnel data with the bench-top calibration of the slot exit velocity vs. the imposed cavity pressure oscillations.

2.3 The 0.3-meter Transonic Cryogenic Wind Tunnel

The experiment was conducted in the 0.3-meter Transonic Cryogenic wind Tunnel at the NASA Langley Research Center. It is a closed loop, fan driven tunnel with a test cross-section of 0.33m by 0.33m. Gaseous nitrogen is the test medium. The tunnel operates at stagnation pressures ranging from 1.2 bar up to six bar and total temperatures from 78K up to 327K[9,10]. A fully automatic control system maintains the test conditions, providing a high level of

repeatability. The floor and ceiling of the tunnel were slightly diverged near the model to reduce blockage resulting from boundary-layer growth on the test section walls. The tunnel sidewalls are parallel, so no divergence is possible in the direction normal to the model surface. In certain runs, a turntable that was instrumented with static pressure orifices was placed opposite the test model in order to evaluate wall interference.

2.4 Oscillatory Blowing System

The Oscillatory Blowing System is capable of generating any desired combination of steady and periodic momentum transfer between the cavity inside the model and the external flow. More details can be found in Ref. 8.

2.5 Bench-Top Experiments

A bench-top calibration was performed in order to correlate the cavity pressure fluctuations (p'_c) with the resulting fluctuating slot velocities ($u'_{j,d}$). This calibration was performed for the x/c=0.59 and x/c=0.64 slots and covered the entire frequency range and most of the normalized amplitude $(p'/\rho)_c$ range that was used in the cryogenic wind tunnel tests. The frequency response of the present excitation system (oscillatory blowing valve-manifold-cavity) is significantly simpler than the one used previously[5]. This allows the generation of a single correlation between $u'_{j,d}$ and $(p'/\rho)_c$ for each slot calibration.

The slot width changed by as much as ±10% (0.05 mm) between different runs due to the modular nature of the model and also due to cryogenic cycling. This is accounted for in the uncertainty level of $\langle c_\mu \rangle$ (i.e. ±25%). More details on the slot calibration are given in References 5, 6, 8.

The frequency response of the unsteady pressure transducers was modified due to the difference in the installation of individual transducers. To quantify this effect, all the transducers underwent a bench-top calibration, prior to installation and as installed in the model, at ambient conditions. This was performed with the model outside the test section as well as when the model was installed in the tunnel. A sound source and a calibrated microphone were placed close to the model. The output of all transducers and the microphone were recorded. The correction procedure is temperature dependent[6] since the resonance frequency is proportional to $\sqrt{T_{windtunnel}/T_{benchtop}}$. Since the majority of the installed sensors resonated at a frequency of about 2.5KHz and the frequency response up to 2KHz was flat, only the flat portion of the frequency range is presently considered.

In certain cases the spectra are normalized by the spectra of the baseline flow at identical tunnel conditions. This eliminates any bias that is sensor or installation related.

2.6 Experimental Uncertainty

Most of the experiments were conducted at cryogenic pressurized conditions (about 100K), close to the lower limit of the tunnel capability. Most of the data were obtained with separated flow regions on or downstream of the model. Table 1 contains the relevant information regarding experimental uncertainties. These values were calculated using ±3 standard deviations of the various experimental conditions and calculated parameters (including repeated runs). All of the test instruments were operated with dated calibration.

Item	uncertainty [of Full scale]	Full scale and condition
Slot width	20%	0.5mm
Static Temperature	0.3%	300K
Static Pressure	0.25%	77 psi
R_c	1%	M>0.2
M	2%	M<0.3
F^+	2%	2
c_μ	0.01 or 10%	the larger
$<c_\mu>$	25%	local values
f	0.3%	800 Hz
C_p	1%	M<0.3
C_p	3%	M=0.65
C_p'	15%	M<0.3
C_p'	30%	M=0.65

Table 1 Uncertainty of flow and control parameters, % of full scale unless otherwise noted.

The uncertainty of the calculated aerodynamic parameters at M<0.3 are listed in Table 2 (in absolute values and related to flow condition on the model):

parameter	baseline	controlled
C_n	0.010	0.015
C_{dp}	0.0005	0.0010
C_m	0.005	0.010

Table 2 Uncertainty of aerodynamic parameters. These values should be roughly doubled for M=0.65 data.

2.7 Experimental Conditions

The experiments were conducted at Mach numbers from 0.20 to 0.70 and chord Reynolds numbers ranging from 2.4×10^6 to 39×10^6.

3. Results

3.1 General

The results presented in this part of the paper are divided into two sections. The first section describes the baseline flow over the model. This section is further subdivided to describe the effects of compressibility and sweep on the baseline flow. The second section describes the controlled flow in compressible and swept (incompressible) flow conditions and the effects of the excitation location. The Reynolds number, the excitation frequency and magnitude, and the effect of steady mass transfer alone or superimposed on the excitation are all considered. Detailed flow field dynamics that are associated with the data are included in the accompanying paper[11].

3.2. Description of the Baseline Flow

3.2.1. Compressibility Effects

Mach number has a significant effect on the flow characteristics over the model, as shown by the integral parameters that are presented in Fig. 4. These data were acquired at three different Reynolds numbers, since the available tunnel test conditions do not allow covering the required Mach number range in a single Reynolds number sweep[9]. However, the Reynolds number was shown to have a very weak effect on the flow over the model, at incompressible speeds, presumably due to the elimination of laminar-turbulent transition[8]. Indeed, the smooth transition of the data between the different Reynolds numbers demonstrates that point also in compressible flow conditions. Consistent, but weak, Mach number effects could be seen at M≤0.6. For higher Mach numbers, C_n, C_m and C_{dp} vary rapidly (Fig. 5). The form drag (pressure and wave) increases four fold between M=0.6 and 0.7, and the quarter chord moment is tripled.

The reason for these changes in the integral parameters become clear when observing the steady and fluctuating wall pressures for $R_c = 30 \times 10^6$ and a range of Mach numbers that are presented in Fig. 6. Table 3 presents several flow indicators corresponding to the data that is presented in Fig. 6.

M	$C_{p,crit}$	$C_{p,min}$	$\Delta C_{p,rec}$
0.600	-1.29	-1.08	-0.56
0.625	-1.14	-1.12	-0.62
0.650	-1.01	-1.29	-0.76
0.675	-0.89	-1.56	-0.93
0.700	-0.78	-1.68	-0.70

Table 3 Several flow indicators of the data shown in Fig. 6.

The flow at x/c<0.2 is insensitive to Mach number. It was noted that the flow acceleration in the range 0.2<x/c<0.5 increases with Mach number. This trend started at M>0.2 (not shown). For M>0.625, the flow around the suction peak is supersonic. The sharp

pressure rise (recovery), centered on x/c=0.6 at all the sub-critical flow conditions, coincides with the location of the shock wave that follows the supersonic flow at M≥0.65. The pressure jump across the shock ($\Delta C_{p,rec}$) increases with M up to M=0.675. Note that C_p at separation decreases as Mach number increases (again this trend starts for M>0.2), indicative of a limit to the baseline flow pressure recovery of about one. The decrease of C_p at separation as Mach number increases is the main cause to the integral parameters divergence, which can be seen in Figures 4 and 5. The negative C_p downstream of reattachment is attributed to tunnel blockage. This is because reattachment, as indicated by the location of $C_{p'max}$, does not change for M<0.675 (Fig. 6). The wall pressures opposite the model (plotted in Fig. 7) show that the tunnel blockage increases significantly for M>0.65. Therefore control was applied at M=0.65, where tunnel wall interference is relatively weak. The shock does not turn the flow subsonic at M=0.7 and a supersonic separation takes place (Fig. 6). Flow reattachment does not change considerably, since the separation is subsonic. For M=0.7 the flow reattaches downstream of the measurement domain and there are indications of buffeting and prohibitively high drag. The effect of Mach number on the fluctuating wall pressures for M<0.675 is weak, as shown in Fig. 6. A small downstream movement of $C_{p'max}$ is indicative of delayed reattachment. The C_p' distribution for M=0.7 differs from the lower Mach number C_p' in that it does not peak around x/c=1.1 but has a lower flat peak centered at x/c≈1.3. An examination of the spectral content at M=0.65 and M=0.7 reveals that the power spectral density at the higher Mach number and $F^+ < 1$ increases by about an order of magnitude without showing any distinctive peak in that F^+ range.

The spanwise distributions of C_p at compressible speeds are presented in Fig. 8. It is noted that for x/c=0 and for x/c=0.95 the pressures are uniform (±0.01) at least over the range z/c=±0.55. For x/c=0.49, the maximum deviation of the local C_p from the mean C_p across the span is ±0.03. This larger deviation can be attributed to minute changes in the contour due to the modular nature of the model as well as cryogenic cycling that are manifested as C_p variations in locally supersonic speeds.

3.2.2. The Effect of the Sweep Angle

The effect of sweep on the baseline and on the controlled flow was studied by rotating the model to a mild sweep angle of Λ=30 deg and repeating the same baseline and controlled flow conditions as in the 2D configuration[8]. The Reynolds number has a very weak effect on the model pressure distributions (Fig. 9), similar to the two-dimensional flow. Note that C_p is

calculated as for 2D flow and x is measured perpendicularly to the reference leading edge. The same orifices were used to measure the wall pressures and the x/c location is maintained, because the major direction of the attached flow development is assumed to be along the chord, regardless of the sweep angle. The spanwise distribution of C_p was monitored and the results for three incompressible Reynolds numbers are presented in Fig. 10. Note that z'/c=rsinφ, where r is the radial distance between a pressure tap and the center of the turntable, located at x/c=0.5 and z=0, and φ is the angle between r and the z=0 axis. The z'=0 axis is the midpoint between the swept end plates and it coincides with the free stream direction. The data presented in Fig. 10 shows an almost spanwise uniform C_p distribution over the range –0.3<z'/c<0.4 (where the streamwise row of pressure taps are located, as indicated by the arrow between the two vertical lines on Fig. 10). The deviations from spanwise uniformity are observed to be a weak acceleration along the leading edge (x/c=0, $\Delta C_p / \Delta(z'/c)$ =-0.08), and a weak deceleration along the trailing edge (x/c=0.95, $\Delta C_p / \Delta(z'/c)$ =0.19) at all Reynolds numbers. An almost perfect spanwise uniformity can be seen at x/c=0.49. A 3D numerical simulation should reproduce the small deviation from spanwise uniformity, undesirable as it is.

The effect of sweep on the efficacy of active separation control was recently studied over a flapped NACA 0018 airfoil at low Reynolds numbers[12]. Various scaling laws were proposed and the effectiveness of separation control using periodic excitation was demonstrated at swept flow conditions. We shall attempt to apply some of the scaling laws to the baseline flow and subsequently will apply it to the controlled flow. Clearly, the scaling for the Reynolds number could not be tested using the present set-up, which is insensitive to R_c.

The effect of sweep on the model baseline pressure distributions is shown in Fig. 11 that compares 2D (Λ=0) and 3D (Λ=30 deg) pressure distributions. In agreement with the reduction of the dynamic pressure along the chord of the swept model, according to $q_{3D} = q_{2D} \cos^2 \Lambda$, the magnitude of the pressure coefficient is reduced over the attached region of the model at the swept flow condition. The flow separates at x/c=0.65, regardless of the sweep angle, and at about the same C_p. The two pressure distributions are almost identical from the separation point to x/c≈0.85. A small difference can be noted in the form of a higher flow acceleration above the bubble in the swept flow. That is indicative of enhanced spreading of the shear-layer due to enhanced mixing. Moreover, the pressure recovery above the bubble, as the flow turns to the surface, is stronger at the swept condition and reattachment occurs

upstream of the 2D reattachment. While the 2D flow reattaches at x/c≈1.2, the swept flow reattaches at x/c≈1.05 (note that $1.05/\cos 30^0 = 1.21$). The fluctuating pressure distributions (also in Fig. 11) show an even more dramatic difference. The $C_p{'}$ immediately downstream of separation are amplified in the swept-flow, and $C_p{'}_{max}$ are more than 50% higher than in the 2D flow. The forward motion of $C_p{'}_{max}$ at the swept flow is in agreement with the upstream motion of the reattachment point. The $C_p{'}_{3D}$'s are lower than their 2D counterparts downstream of reattachment, as seen in 2D flow where reattachment moved forward due to effective control. Clearly, scaling the swept C_{p3D} and

$C_p{'}_{3D}$ by a single factor, i.e. $\cos^2 \Lambda$, would not collapse the two pressure distributions that are presented in Fig. 11. The suggested simple scaling sub-divides the flow into two regions: the attached flow C_p (i.e. x/c<0.64), which is normalized by $\cos^2 \Lambda$, and the separated flow region (i.e. x/c>0.65), where the chord is normalized by $\cos \Lambda$ (i.e. assuming that the flow development is along the external flow direction). The result of this scaling is presented in Fig. 12. It can be observed that the scaling for the attached flow is only partially successful. It under corrects at x/c<0 and at 0.2<x/c<0.6. This disagreement with the conventional scaling could not be attributed to poor simulation of "infinite" swept flow since the spanwise uniformity is very good at this region. The scaling for the separated and reattached flow is to plot C_p vs. $x/(c \cos \Lambda)$ and this collapses the pressure distributions over the bubble very well. The location of $C_p{'}_{max}$ for both the sweep angles became closer, but the differences in the level of $C_p{'}_{3D}$ remained. It was shown[13] that the spanwise velocity fluctuation (w') grows very rapidly under an adverse pressure gradient in 3D flow, and the magnitude of w' is similar to that of u' as incipient separation develops. This is an indication that the total turbulence level in 3D separation would be larger by a factor of about $\sqrt{2}$ as compared to the turbulence level in 2D flow. The same reference notes that w' is mainly active near the wall while u', which is a remnant of the upstream-attached layer, is mainly active above it. The two layers merge at reattachment.

3.3. Controlled Flow over the "Hump" Model
3.3.1 General
This section is devoted to a description of the controlled flow over the model. Since the baseline flow contains separated flow, there is no attached baseline flow to be used as a reference. Strong suction was applied in order to reattach the flow at low Mach numbers and it was used to study fully attached 3D flow conditions and examine various scaling laws. At compressible speeds, the available suction or blowing levels were insufficient to fully reattach the flow, or at least demonstrate

saturation of the effect, but the efficacy of similar momentum coefficients could be compared at different Mach numbers. Thereafter, periodic excitation was used to control the size of the separation bubble and gradually eliminate it. The parameters that were modified during the test are the frequency and the amplitude of the periodic excitation, and the magnitude of the steady mass flux. Additional geometrical parameters were the slot location and the sweep angle. The effects of the Reynolds and Mach numbers were also studied. The spanwise uniformity of the mean wall pressures was found to be very good and generally improved with the application of periodic excitation, regardless of the sweep angle. The effect that the upstream boundary layer thickness has on the baseline and on the controlled 3D flow is small and will not be discussed here in detail.

3.3.2 Compressibility Effect on Separation Control
The location of the shock wave at compressible speeds coincides with the location of the steep adverse pressure gradient at the highly convex area of the model that causes separation at low Mach numbers. At M=0.65 the shock turns the flow subsonic just upstream of separation, since $C_{p,crit} = -1.01$. The length of the baseline bubble at M=0.65 is only slightly longer than its length at M=0.25. The lengthening of the bubble is an indication of the lower mixing rate in the compressible shear-layer, since the mixing rate determines the rate at which the separated shear layer approaches the wall. The range of available reduced frequencies, based on the length of the bubble (taken here also as c/2) and on the free stream velocity is 0.15 to 0.6. A range of these frequencies was scanned at oscillatory momentum coefficient of $\langle c_\mu \rangle = 0.055 \pm 0.005$ (see Fig. 13), and indicates that $F^+ = 0.6$ is the most effective tested frequency for shortening the bubble. The receptivity of the separated shear layer, as indicated by $C_p{'}$ at x/c=0.67, is not frequency dependent, but $F^+ = 0.6$ is the most amplified above the bubble. Only a very weak unsteady upstream effect (i.e. at x/c=0.2) of excitation is observed at M=0.65. This is different from our findings for low Mach number using low F^+ [Ref. 8, Fig. 13a]. The reason for this effect is that the upstream acoustic propagating wave cannot affect the region that is upstream of a supersonic flow.

The effect of increasing the magnitude of the excitation on the efficacy of active separation control at M=0.65 is presented in Fig. 14. The strength of the shock wave increases with the excitation level, the bubble gets shorter and $C_p{'}_{max}$ increases and moves upstream. Again, the unsteady excitation is not sensed upstream of the supersonic region (not shown), at x/c=0.2 since $C_p{'}$ there is unchanged. An indication to the effectiveness of active separation control at

6
American Institute of Aeronautics and Astronautics

different Mach numbers can be obtained by evaluating the reduction in the length of the bubble for a given $<c_\mu>$. This was performed by comparing mean and fluctuating pressures generated by $F^+=0.6$ at M=0.65 with those generated by $F^+=0.8$ at M=0.25 (Fig. 15). The bubble pressure coefficients were normalized in the following manner:

$$C_{p,n} = \frac{C_p - C_{p,R,b}}{C_{p,S,b} - C_{p,R,b}} \qquad (1)$$

to enable a clearer comparison. The effect of this scaling on the baseline bubbles can be seen in Fig. 16a (C_p's were not scaled). The scaling shows a slightly longer bubble at M=0.65. The same scaling was applied to the controlled bubble C_p (Fig. 16b). While at M=0.25 $C_{p,S}$ increased due to the control, at M=0.65 $C_{p,S}$ is unchanged. The initialization of the pressure recovery is at x/c=0.75 for M=0.25 and at x/c=0.9 for M=0.65. A three fold increase in $C_{p,max}'$ (compared to $C_{p\,max,b}'$) and a forward movement of $C_{p\,max}'$ to x/c= 0.8 can be observed at M=0.25 while at M=0.65 $C_{p\,max}'$ increases by a factor of two and it moves only to x/c=1.05. It could be stated that at compressible flow conditions, periodic excitation is less effective than in incompressible flow, at least in shortening the bubble using low F^+ that is introduced from the x/c=0.65 slot. As will be shown in the following section, the effectiveness of steady mass-flux to shorten the bubble is also reduced at M=0.65.

Steady mass-flux was applied to control separation at compressible speeds and its effectiveness is evaluated at M=0.25 and 0.65 and compared to the efficacy of unsteady excitation. Figure 17 presents the mean and fluctuating wall pressure distributions at M=0.65 due to the application of steady blowing. Hardly any response can be seen for blowing at $c\mu$ <0.2%, as for low Mach numbers. For $c\mu$ >0.2%, separation moves downstream, increasing the strength of the shock wave. Reattachment does not move forward, as C_p' does not increase and $C_{p\,max}'$ stays at the same location. Steady suction was also used and the corresponding pressure distributions are presented in figure 18. The response to steady suction is gradual and is mainly manifested as shortening of the bubble through increased flow unsteadiness and increased wall pressure fluctuations downstream of separation. The strength of the shock wave increases, presumably due to the suction that induces acceleration upstream of the slot. The pressure at separation does not change considerably. Reattachment moves upstream as indicated by the upstream movement of $C_{p\,max}'$ and the beginning of the pressure recovery.

Figure 19a presents a comparison of steady and periodic mass transfer effects on the aerodynamic moment coefficient measured at M=0.25 and M=0.65.

Similar trends could be seen in the moment data regardless of Mach number. Suction is more effective than blowing in modifying the moment and the response is gradual over the entire c_μ range. The moment is mainly indicative of shortening of the bubble and its modification is important for control purposes. Figure 19b presents the effect of compressibility on the modification of the pressure drag by steady and periodic momentum transfer. Since the form drag is mainly affected by changes in the pressures on the highly sloped areas of the model, one should not be surprised to find that the form drag at M=0.65 is not affected as it was at M=0.25. Suction is not effective for reducing the form-drag since the mean pressure at separation does not increase with the increase in c_μ (Figure 18). Blowing is more effective for reducing the form-drag since the pressures at separation increase with the blowing c_μ (Figure 17). Furthermore, blowing generates a favorable effect for $c\mu$ <0.1% while at low Mach numbers it becomes effective only for $c\mu$ >0.2%.

The modification of the integral parameters due to the application of periodic excitation are compared to the effects due to the application of steady mass flux in Figs. 19a and 19b. The compared reduced frequencies, $F^+=0.4$ at M=0.25 and $F^+=0.3$ at M=0.65, are located near the lower limit of the effective frequencies for separation control. The data indicates that periodic excitation using low F^+ is as effective as steady suction in modifying the moment at compressible speeds, while it was less effective at M=0.25. The reduced frequency $F^+=0.3$ (M=0.65) follows the form-drag blowing data very closely, while steady suction is ineffective in modifying C_{dp} at M=0.65. A Comparison of pressure distributions measured in the presence of periodic excitation with those generated by the application of steady mass-flux, using the same C_p's (<0.1%, data not shown) indicates that both $F^+=0.3$ and 0.6 are more effective in shortening the bubble than steady suction. At blowing levels that are comparable to the available $\langle c_\mu \rangle$, steady blowing is entirely ineffective. Additional data that considers the effects of F^+ at M=0.65 will be discussed in section 3.3.4.

3.3.3 Swept Controlled Flow

The swept baseline flow contains a large turbulent separation bubble, as in the 2D flow. Therefore, steady suction or blowing was applied to gradually reattach the flow to the surface of the model. The effectiveness of steady mass-flux in modifying the flow is compared in the 2D and 3D flows. Steady suction was applied from the x/c=0.59 slot, and the effects on the moments and form drag coefficients are shown in Fig. 20 for Λ=0 deg and Λ=30 deg. The data indicates that the gradual

reduction in C_{dp} and the concomitant increase in C_m do not deteriorate for the swept flow, especially for $c_\mu > 0.1\%$.

The data shown in Fig. 21 demonstrates the effectiveness of steady suction and periodic excitation in modifying the form drag on the model at the two sweep angles when control is applied from the x/c=0.64 slot. Note the increased effectiveness when the control is applied from the x/c=0.64 slot, compared to its effectiveness when applied from the x/c=0.59 slot (Fig. 20). The data indicates that for steady suction as well as for periodic excitation, the drag reduction is larger in the swept flow but the rate of drag reduction is smaller. The data at $F^+ = 2$ and $\Lambda = 0$ deg (Fig. 21) agrees very well with the lower F^+ data (not shown). The swept data at $F^+ = 2$ behaves differently. It reduces the drag more for low $\langle c_\mu \rangle$'s and less for higher $\langle c_\mu \rangle$'s.

Fig. 22 compares pressure distributions with suction $c_\mu \cong 0.5\%$ applied from the x/c=0.64 slot for $\Lambda = 0$ and $\Lambda = 30$ deg. The form drag corresponding to both pressure distributions is nullified by the suction. Note that the swept pressure coefficient is scaled according to $C_p = C_{p3D}/\cos^2 \Lambda$. The data clearly shows that suction at $c_\mu \cong 0.5\%$ has a comparable effect on the flow regardless of the sweep angle and that the conventional scaling works very well for this partially attached flow. The C_p's are in very good agreement without any scaling, so if q_{3D} should be used to scale $C_p'_{3D}$ the conclusion would be that it increased by a third in comparison to its 2D counterpart, in agreement with the higher $C_p'_{3D}$ of the baseline 3D separation bubble.

Fig. 23 presents the form drag variation at the two sweep angles due to the application of periodic excitation using $F^+ = 0.8$ and $F^+ = 1.6$ with increasing $\langle c\mu \rangle$. Note that the baseline form drag is presented for $\langle c\mu \rangle = 0.001\%$, for both sweep angles. It can be seen that the sensitivity to F^+ is weak regardless of the sweep. While at $\Lambda = 0$ deg periodic excitation with $\langle c\mu \rangle < 0.02\%$ increases the form-drag, at $\Lambda = 30$ deg periodic excitation at $\langle c\mu \rangle < 0.02\%$ is neutral. The effectiveness of periodic excitation using $\langle c\mu \rangle > 0.02\%$ is similar for both sweep angles.

Fig. 24 compares pressure distributions with periodic excitation that is applied from the x/c=0.64 slot using $\langle c\mu \rangle \cong 0.2\%$ and $F^+ = 2$. Note that the swept $C_p = C_{p3D}/\cos^2 \Lambda$ collapses the two data sets very well, indicating again that this scaling works well also

for partially attached flow. The 2D and 3D fluctuating wall pressures (C_p') are in good agreement, without any scaling, consistent with the current findings for reattached flow using steady suction.

The dynamic pressure at the swept flow is reduced according to $q_{3D} = q_{2D}\cos^2 \Lambda$, therefore it was suggested[12] that the integral parameters for the swept flow should scale according to

$$C_{dp3D} = C_{dp2D}/\cos^2 \Lambda \qquad (2)$$

and

$$C\mu_{3D} = C\mu_{2D}/\cos^2 \Lambda \qquad (3)$$

The swept flow data of Fig. 21 and Fig. 23 are re-plotted in Figs. 25 and 26 when the form drag and the momentum coefficients are scaled according to Eq. 2 and 3. The data clearly shows that when the control overcomes the massive separation, using steady suction with $C_\mu > 0.1\%$ or periodic excitation with $C_\mu > 0.2\%$, the conventional scaling works very well. As long as the flow encloses a massively separated flow region, the conventional 3D scaling fails to collapse the data to a single curve. This is in agreement with the finding that the conventional scaling fails to collapse the pressure distributions that are associated with the bubble.

3.3.4 Effects of Excitation Slot Location

The effect of the relative location between the excitation slot and the boundary layer separation was studied using two alternative blowing slot locations, i.e. x/c =0.59 and x/c =0.64 at M=0.25 and M=0.65 for sweep angles of $\Lambda = 0$ and $\Lambda = 30$ degrees. Separation always occurred at x/c=0.65, regardless of the Reynolds number, Mach number or the sweep angle. It was previously shown[8] that the location of the blowing slot did not alter the baseline separation to a measurable extent, at low Mach numbers, but it did effect the shock wave and the separation at compressible speeds, as will be shown here.

A range of steady suction rates was applied from both slots at M=0.25, $R_c = 21 \times 10^6$ and 2D flow. The data that is shown in Fig. 27, indicates that when suction is applied from the x/c=0.59 slot it has a gradual, but small, effect on the integral parameters. Suction that is applied from the x/c=0.64 slot has a negligible, or even detrimental, effect on C_{dp} for $c\mu < 0.1\%$. The form drag is gradually and very effectively eliminated using higher suction levels ($C_{dp} = 0$ for $c\mu \sim 0.6\%$) that are applied from the x/c=0.64 slot.

The effect of the slot location on the efficacy of periodic excitation ($F^+ = 0.8$) or steady suction, with increasing $C\mu$, in reducing the form drag, is shown in Fig. 28. The data indicates that introducing periodic excitation from the x/c=0.59 slot increases the form drag for the entire available range of $< c_\mu >$s, while

steady suction that was introduced from the x/c=0.59 slot has a weak but favorable effect of drag reduction (Fig. 27), which is presumably due to thinning of the boundary layer upstream of separation. Introducing periodic excitation from the x/c=0.64 slot is significantly more effective than introducing it from the x/c=0.59 slot. It has a similar, though weaker, effect to steady suction that is applied from the x/c=0.64 slot. The great sensitivity to only 5%c change in the location of the excitation slot is attributed to the highly curved surface in the separation region.

Baseline and controlled C_p and C_p', where periodic excitation with $\langle c_\mu \rangle \approx 0.06\%$ emanates from either one of the slots, are presented in Fig. 29a. The baseline pressure distributions indicate that while the x/c=0.59 slot (its location indicated by a thick dashed-dotted line) is located at the beginning of the baseline pressure recovery, the x/c=0.64 slot (thick dashed line) is located just upstream of separation. The data shows that low amplitude excitation (Fig. 29a) promotes earlier separation, as indicated by the slightly lower C_p at x/c=0.65, regardless of the active slot location. The x/c=0.64 excitation causes immediate turning of the shear-layer towards the wall, while the x/c=0.59 excitation increases the spreading rate of the shear layer (since the flow above the bubble continues to accelerate). This is accompanied by a very rapid amplification of the wall C_p' (for 0.65<x/c<0.8). The pressure recovery of the excited flow using the x/c=0.59 slot for x/c>0.75 is stronger. This leads to reattachment at similar locations, about one separation height downstream of the secondary $C_p'_{max}$ that is positioned at x/c=0.8. When the excitation emanates from the x/c=0.59 slot, its upstream effect is stronger. Significant differences in the effectiveness of high amplitude periodic excitation, using $\langle c\mu \rangle = 0.38\%$ that emanates from the two alternative excitation slots, can be seen in Fig. 29b. A six fold increase in the magnitude of the excitation has very little effect on the average controlled C_p when the excitation is introduced from the x/c=0.59 slot. Since the excitation was introduced 5-6% of the chord length upstream of separation, the excitation level decayed considerably in the attached region of the boundary layer. The special resolution of the unsteady pressure transducers is too coarse to quantify this effect. The x/c=0.64 excitation has almost twice the magnitude of the x/c=0.59 excitation immediately downstream of separation (i.e. x/c=0.67). Separation is delayed using the x/c=0.64 excitation, causing not only a thinner bubble (since separation occurs further downstream on the highly sloped area at the aft region of the model) but also a shorter bubble. Again, the unsteady upstream effect of the excitation is stronger when the x/c=0.59 slot is used.

The effects of steady suction with $c_\mu \sim 0.5\%$ that is applied from the two slot locations are shown in Fig. 30. Suction at $c_\mu \sim 0.5\%$ accelerates the flow upstream of the active slot, regardless of its location. While suction that is applied from the x/c=0.59 slot removes a thin boundary layer, the slot at x/c=0.64 helps the thicker turbulent boundary layer overcome the separation ordained convex area. Interestingly, the flow downstream of the x/c=0.64 slot continues to decelerate when suction is applied. This will presumably be the case as long as the unsteady stagnation downstream of the slot is not brought up to the rear edge of the slot. At a suction of $c_\mu \sim 0.5\%$ only a very small separation bubble exists between 0.7<x/c<0.8. Reattachment occurs at x/c=0.85 and 1.0 respectively, inferring from the location of $C_p'_{max}$. These results suggest that suction will be very effective in separation control when applied immediately downstream of highly convex areas. The incompressible data that was presented in this section clearly shows that control should be applied upstream of separation and as close as possible to it, regardless of the control method. This is especially important on small radius of curvature convex surfaces.

The mere presence of a slot alters the shock wave and separation at compressible speeds (Fig. 31). The x/c=0.59 slot, that is positioned immediately under the mean shock position, causes an unsteady motion in the shock position (indicated by the increased unsteadiness at x/c=0.45) that is manifested as weaker pressure recovery across the shock and separation at a lower C_p. The introduction of periodic excitation from the x/c=0.59 slot, with identical F^+ and $\langle c_\mu \rangle$, is significantly superior to its introduction from the x/c=0.64 slot (Figs. 32a and 32b). The increased upstream suction peak, the increased C_p' downstream of the slot, the reduced C_p' upstream of the slot, the upstream motion of $C_p'_{max}$ and the healthier pressure recovery above the bubble, indicate increased effectiveness of the excitation introduced under the shock rather than downstream of it.

4. Conclusions

Active separation control was applied to a carefully documented baseline flow at high Reynolds numbers. This paper describes several effects of compressibility, sweep and excitation slot location on the baseline and on the controlled flow. The baseline flow is fully turbulent so that laminar-turbulent transition does not baffle the data trends due to the active separation control. The Reynolds number has a very weak effect on the model pressure distributions, regardless of Mach number or the sweep angle.

The effectiveness of the blowing slot located at x/c=0.64 is significantly higher than the slot located at x/c=0.59 at low Mach numbers. This is because the magnitude of the excitation decays considerably in the attached region of the boundary layer, since separation takes place at x/c≈0.65 regardless of the sweep angle. At compressible speeds, the presence of the x/c=0.59 excitation slot alters the pressure distributions. However, the effectiveness of the x/c=0.59 slot, that is located under the shock wave, is greater than that located at x/c=0.64, just downstream of the shock. The shock wave location and the separation line are very close on the present geometry. This eliminates the possibility of introducing the excitation downstream of the shock and still upstream of separation.

The spanwise uniformity of the wall pressures, at unswept flow conditions, was found to be very good and improved as the separation was controlled. The swept flow did not differ considerably from "infinitely" swept flow conditions. Steady as well as periodic control improved the spanwise uniformity at the lee side of the model.

Compressibility tends to elongate the separation bubble due to reduced mixing above the separated shear-layer. Sweep shortens the bubble and significantly increases the level of the wall pressure fluctuations upstream of reattachment, in agreement with other experimental data for incipient 3D separation. The attached flow boundary layer develops in a direction perpendicular to the leading edge and scales, as expected, with $1/\cos^2 \Lambda$, where Λ is the sweep angle, while the separated shear-layer develops along the free stream direction and scales with $x' = x / \cos \Lambda$.

Active control using periodic excitation is comparable to steady suction and significantly more effective than steady blowing, also at compressible speeds, as long as the modification of the integral parameters is considered. The capability of periodic excitation to shorten the separation bubble is reduced at compressible speeds, using similar reduced frequencies and excitation levels. The efficacy of frequencies with $F^+ \approx 1$ to reattach separated flow is maintained in the 3D flow. It was demonstrated that the form drag and the momentum coefficients of the control input scale according to the conventional swept flow scaling $(1/\cos^2 \Lambda)$ when the flow is mostly attached.

References

1. Betz, A. "History of boundary layer control in Germany", p.2. in Boundary layer and flow control, Vol. 1, Ed. By Lachman, Pergamon Press, 1961.
2. Nishri, B. and Wygnanski, I., "The effect of periodic excitation on turbulent flow separation from a flap", AIAA Journal, Vol. 36, No. 4, April 1998, pp.547-556.
3. Seifert, A., Bachar, T., Koss, D., Shepshelovich, M. and Wygnanski, I., "Oscillatory Blowing, a Tool to Delay Boundary Layer Separation", AIAA Journal, Vol. 31, No. 11, 1993, pp. 2052-2060.
4. Seifert, A., Darabi, A. and Wygnanski, I., "On the delay of airfoil stall by periodic excitation", Journal of Aircraft, Vol. 33, No. 4, 1996, pp. 691-699.
5. Seifert, A. and Pack, L.G., "Oscillatory Control of Separation at High Reynolds Numbers", AIAA J. Vol. 37, No. 9, Sep. 1999, pp. 1062-1071.
6. Seifert, A. and Pack, L.G., "Suppression of Shock-induced Separation by Oscillatory Excitation", (AIAA paper 99-0925), submitted to J. Aircraft, March 1999.
7. Murthy, A.V., Johnson, C. B., Ray, E. J., Lawing, P. L., Thibodeaux, J. L., "Studies of Sidewall Boundary Layer in the Langley 0.3-Meter Transonic Cryogenic Tunnel With and Without Suction", NASA TP-2.096, 1983.
8. Seifert, A. and Pack, L.G., "Active Control of Separated Flows on Generic Configurations at High Reynolds Numbers (Invited)", AIAA paper 99-3403, 30th AIAA Fluid Dynamics Conference, Norfolk, VA, June 1999.
9. Ladson, C. A. and Ray, E. J., "Evolution, Calibration, and Operational Characteristics of the Two-dimensional Test Section of the Langley 0.3-meter Transonic Cryogenic Tunnel", NASA TP-2749, 1987.
10. Rallo, R. A., Dress, D. A., and Siegle, H. J. A., "Operating Envelope Charts for the Langley 0.3-meter Transonic Cryogenic Wind Tunnel", NASA TM-89008, 1986.
11. Pack, L.G. and Seifert, A., "Dynamics of Active Separation Control at High Re number Turbulent Flows", AIAA paper 00-0409, Jan. 2000.
12. Naveh, T. Seifert, A., Tumin, A. and Wygnanski, I., 1998, "Sweep Effect on the Parameters Governing the Control of Separation by Periodic Excitation", J. of Aircraft. Vol. 35, No. 3, pp. 510-512.
13. Van der Berg, B. and Elsenaar, A., "Measurement in a Three-Dimensional Incompressible Turbulent Boundary layer in an Adverse Pressure Gradient under Infinite Swept Wing Conditions", NLR TR 72092 U, 1972.
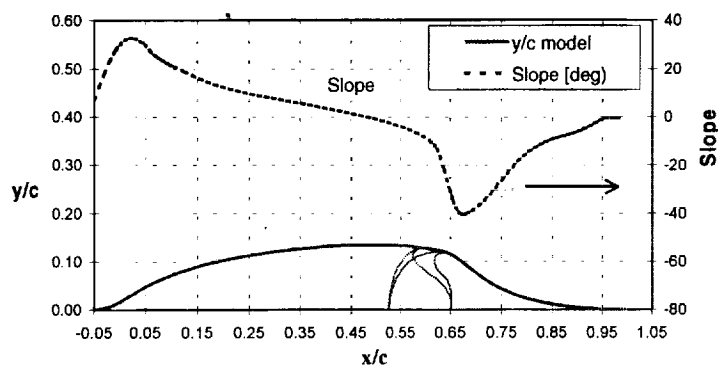
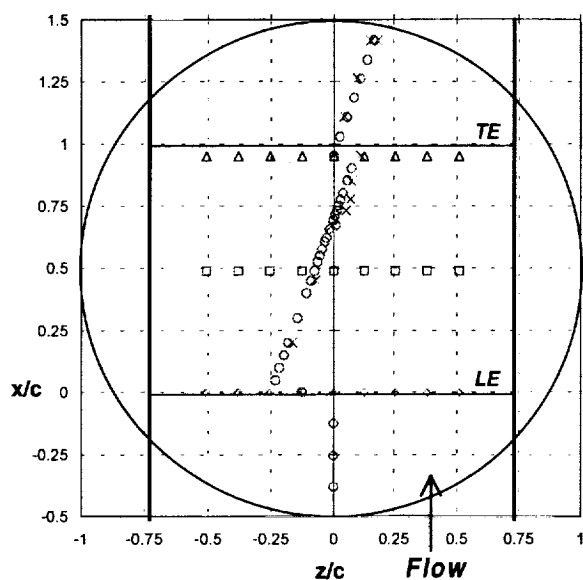**Fig. 1** Cross section of the wind tunnel model, as mounted on the tunnel sidewall.

Fig. 2 Top view of the unswept model. The thick vertical lines indicate the location of the end plates.
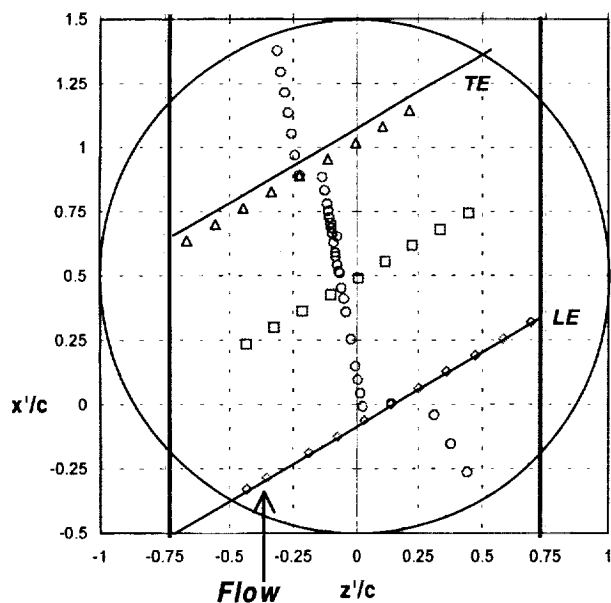

Fig. 3 Top view of the swept model. The thick vertical lines are the end plates.
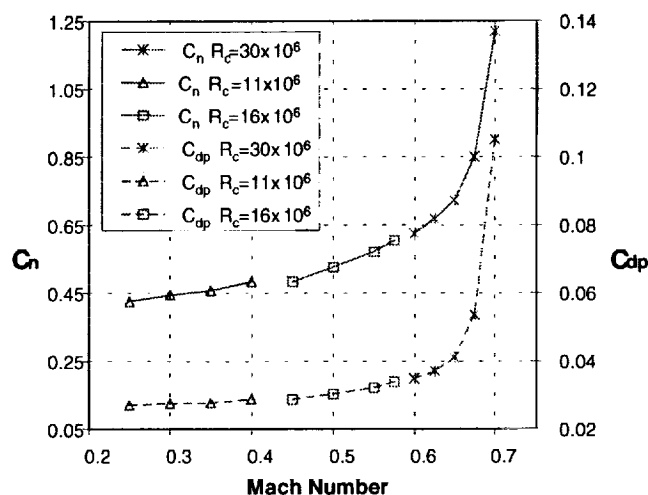

Fig. 4 Integral parameters of the model at compressible 2D flow, R_c in millions.
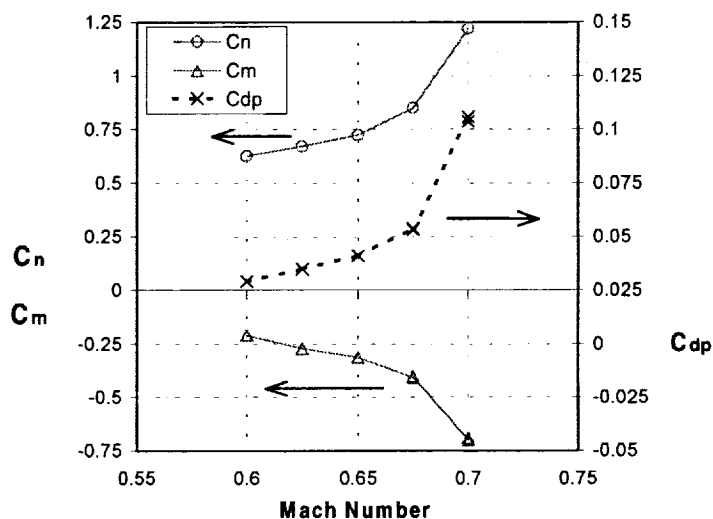

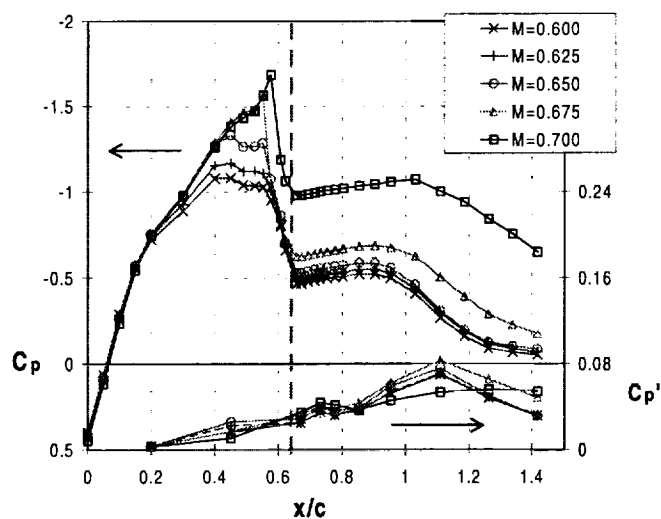**Fig. 5** Integral parameters of the model at compressible 2D flow, $R_c = 30 \times 10^6$.

Fig. 6 Mean and fluctuating wall pressures at compressible 2D flow, $R_c = 30 \times 10^6$.

11

American Institute of Aeronautics and Astronautics
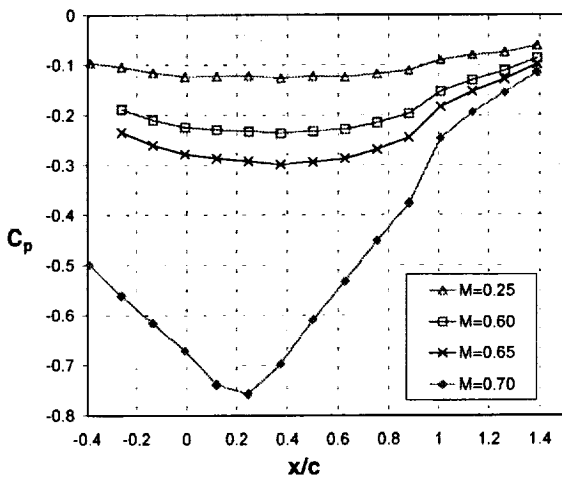
Fig. 7 Mean pressures on the wall opposite the model at compressible 2D flow, $R_c = 30 \times 10^6$.
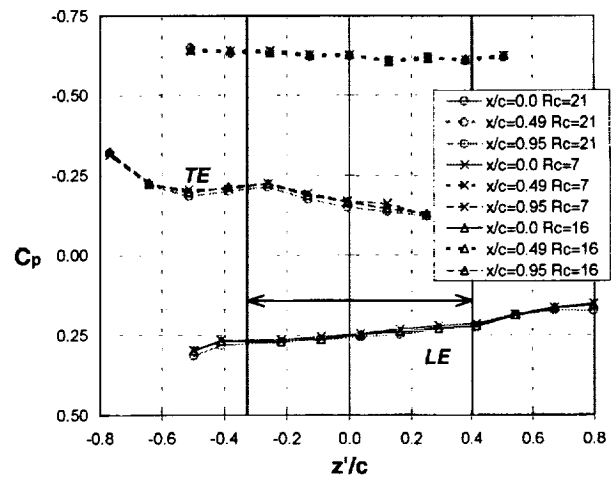
Fig. 10 Spanwise distribution of the model Cp, $\Lambda = 30$ deg, M=0.25.
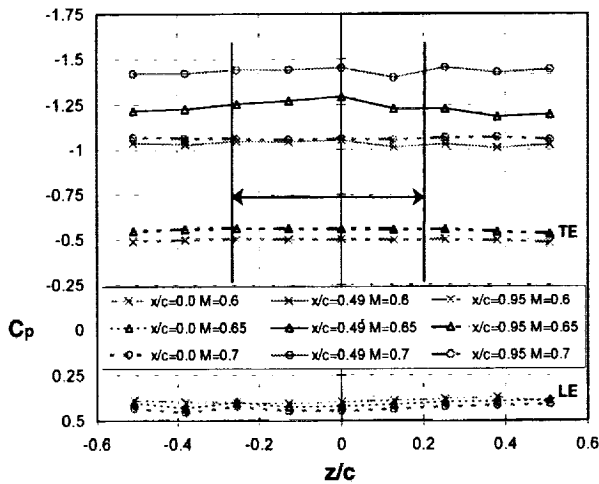
Fig. 8 Spanwise distribution of Cp on the model at compressible 2D flow, $R_c = 30 \times 10^6$.
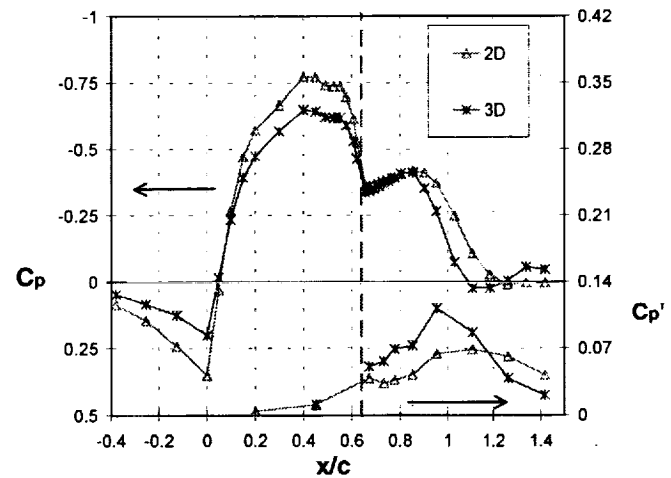
Fig. 11 A comparison of pressure distributions for zero and 30 deg sweep angles, M=0.25, $R_c = 16 \times 10^6$
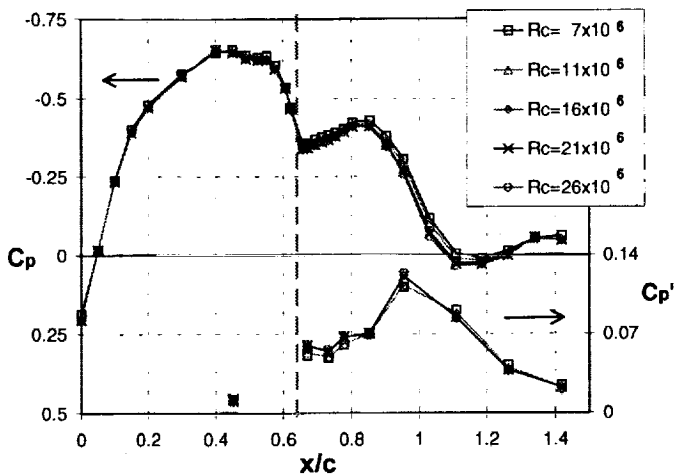
Fig. 9 Swept flow mean and fluctuating wall pressures, M=0.25, R_c indicated in legend.
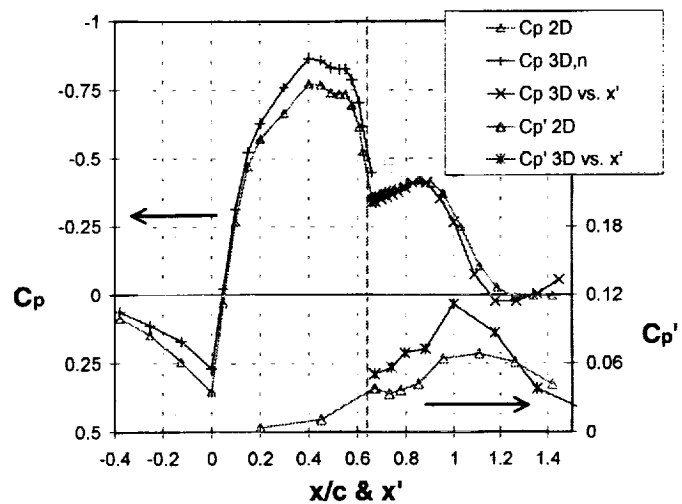
Fig. 12 Scaling of pressure distributions for zero and 30 deg sweep angles, M=0.25, $R_c = 16 \times 10^6$, see text for notation.
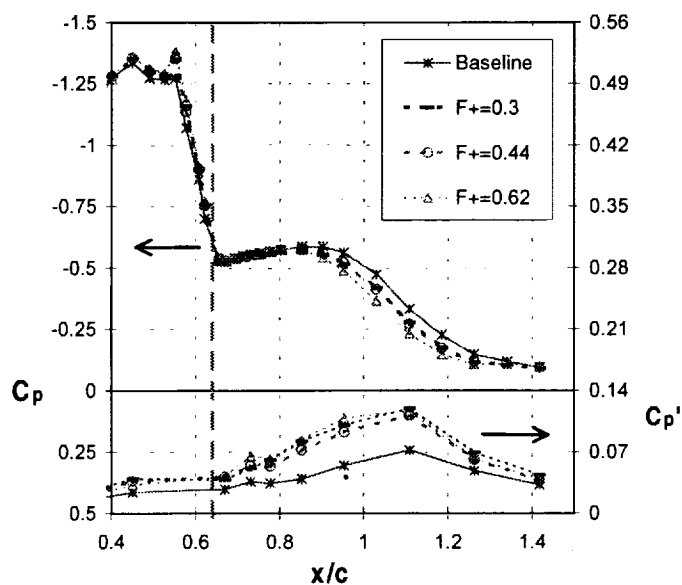
Fig. 13 Baseline and controlled 2D pressure distributions, M=0.65, R_c= 30x10^{6}, <cμ>=0.055%, frequency effect.

Fig. 14 Baseline and controlled 2D pressure distributions, M.=0.65, R_c= 30x10^{6}, F[+]=0.3, amplitude effect.

Fig. 15 A comparison of baseline and controlled 2D pressure distributions, M=0.65, R_c= 30x10^{6}, F[+]=0.3 and M=0.25, R_c= 16x10^{6}, F[+]=0.4.
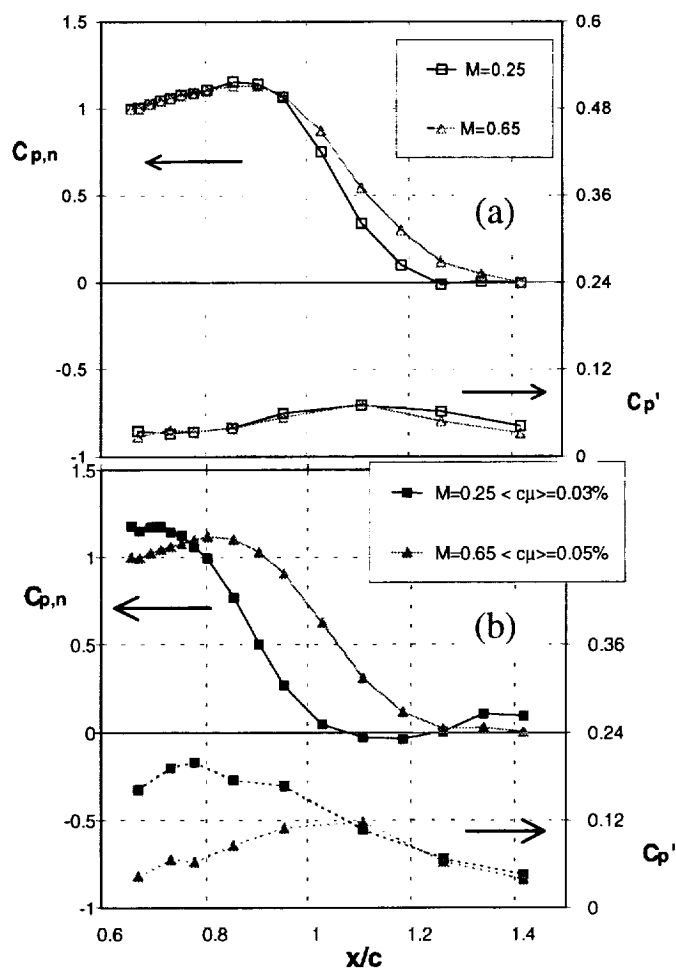
Fig. 16 A comparison of baseline, (a) and controlled, (b) 2D pressure distributions, M=0.65, R_c= 30x10^{6}, F[+]=0.3 and M=0.25, R_c= 16x10^{6}, F[+]=0.4.
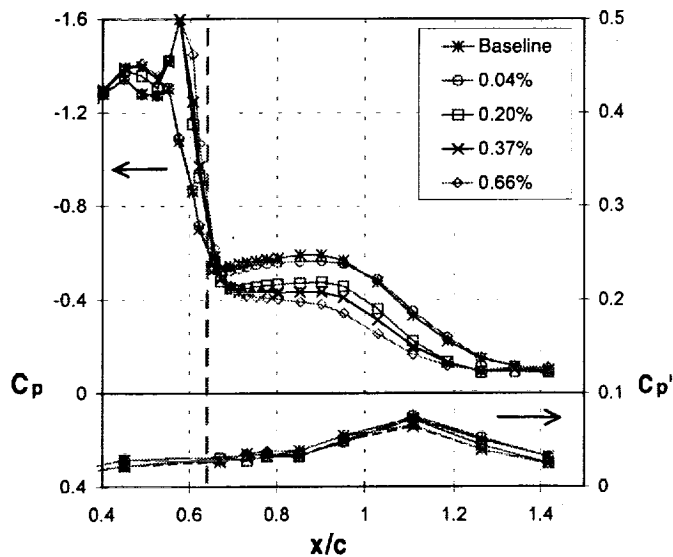
Fig. 17 The effect of steady blowing on the 2D pressure distributions, M=0.65, R_c= 30x10^{6}, slot x/c=0.64. Cμ in legend.
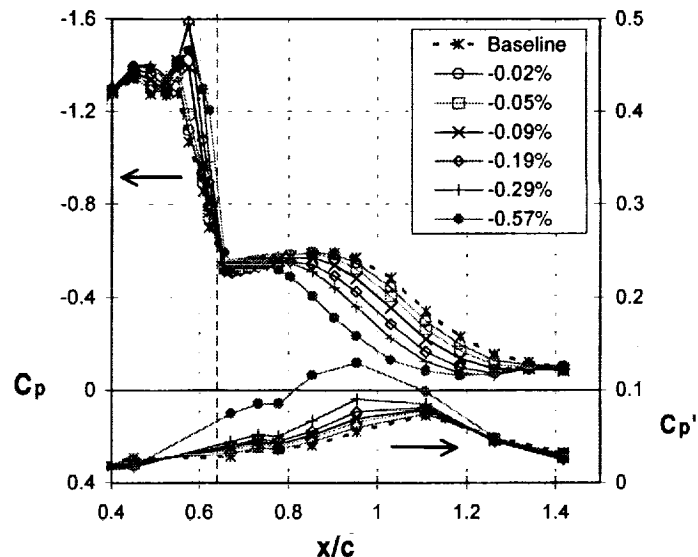
Fig. 18 The effect of steady suction on the 2D pressure distributions, M=0.65, R_c= 30x10^{6}, slot x/c=0.64. Cμ in legend.

(a)

(b)
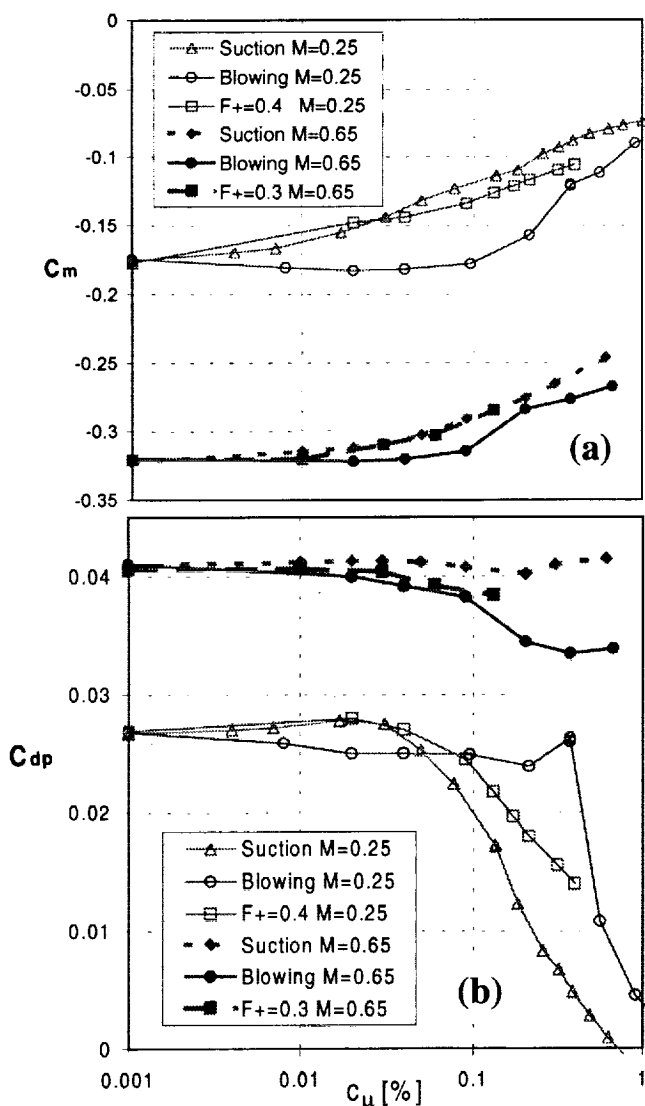
Fig. 19 The effect of steady and periodic momentum addition on the 2D integral parameters, M=0.65, R_c= 30x10^{6}, and M=0.25, R_c= 16x10^{6}, x/c=0.64 slot: moment coefficient (a), form drag (b).
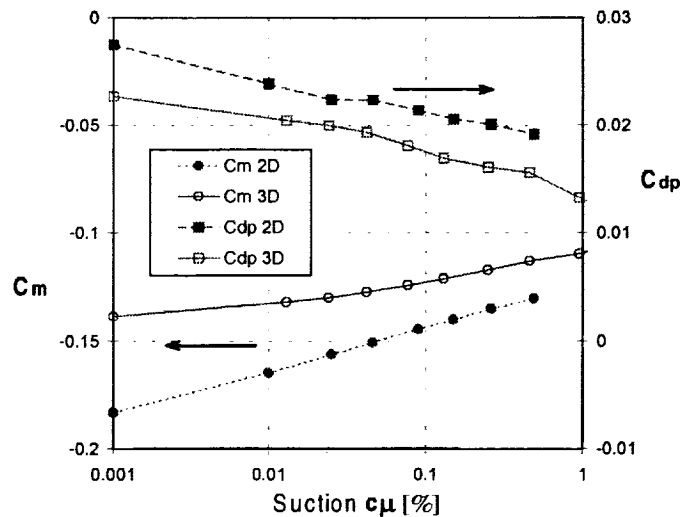
Fig. 20 The effect of sweep on the effectiveness of steady suction as indicated by the moment and form-drag coefficients, M=0.25, R_c= 21x10^{6}, x/c=0.59 slot.
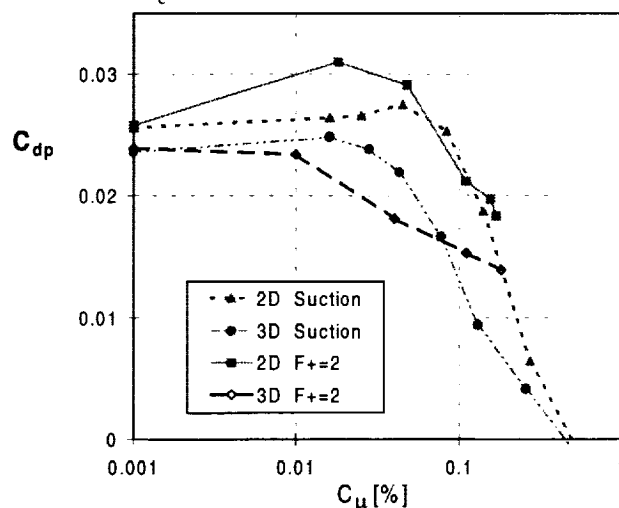
Fig. 21 The effect of sweep on the form-drag coefficients using steady suction or periodic excitation for control, M=0.2, R_c= 17.5x10^{6}, x/c=0.64 slot.

14
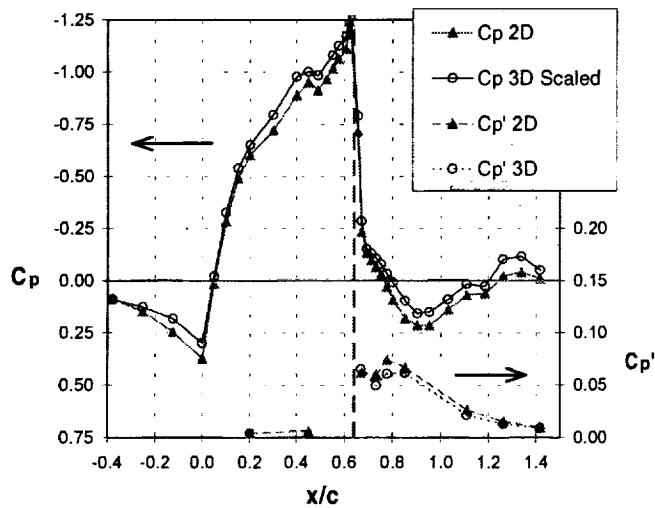
Fig. 22 The effect of sweep on the scaled Cp using steady suction for control, M=0.25, R_c= 21x10^{6}, x/c=0.64 slot, cμ=-0.5%.
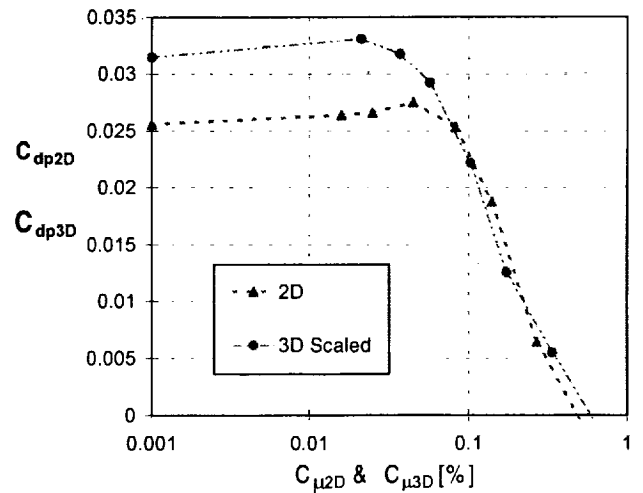
Fig. 25 The effect of sweep on the scaled form-drag using steady suction for control, M=0.25, R_c= 21x10^{6}, x/c=0.64 slot.
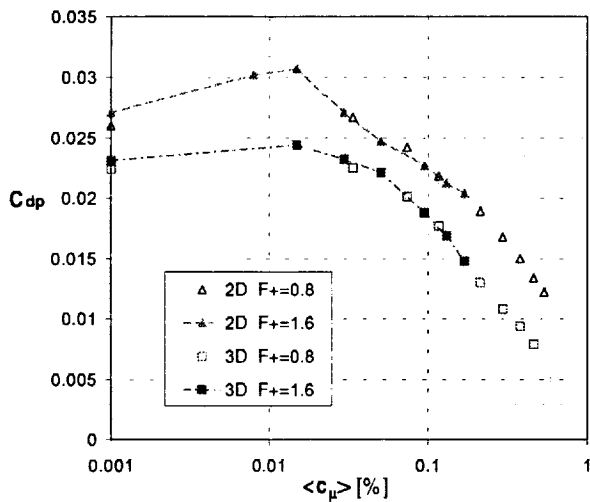
Fig. 23 The effect of sweep on form-drag reduction using F[+]=0.8 and 1.6 for control, M=0.25, R_c= 16x10^{6}, x/c=0.64 slot, cμ=0.
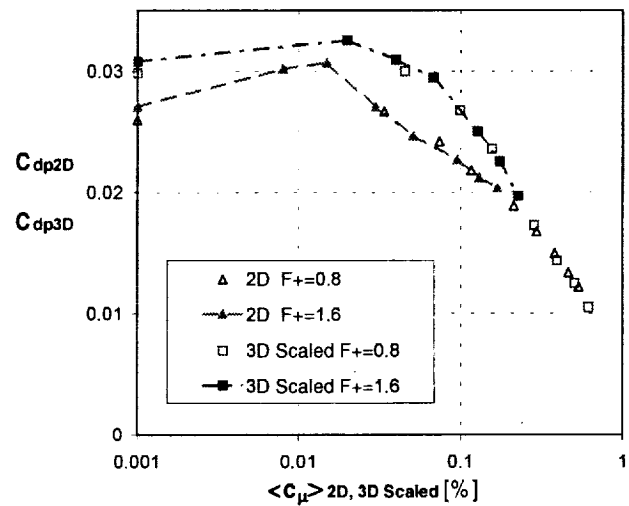
Fig. 26 The effect of sweep on the scaled form-drag using F[+]=0.8 and 1.6 for control, M=0.25, R_c= 16x10^{6}, x/c=0.64 slot, cμ=0.
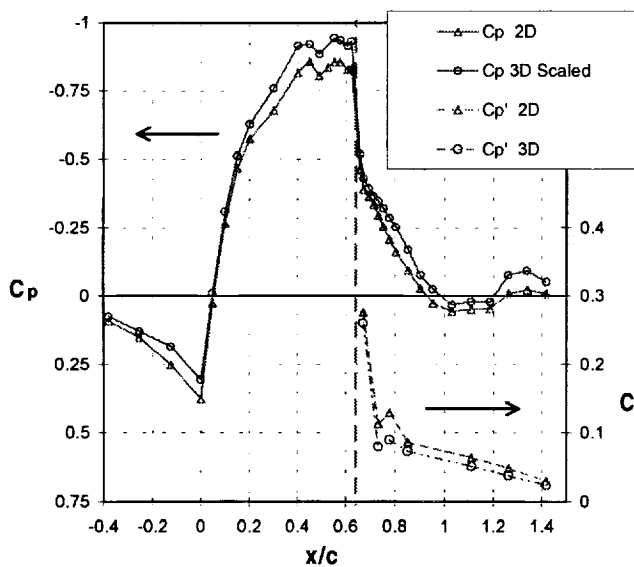
Fig. 24 The effect of sweep on the scaled Cp using F[+]=2 and <cμ>=0.2% for control, M=0.25, R_c= 17.6x10^{6}, x/c=0.64 slot, cμ=0.
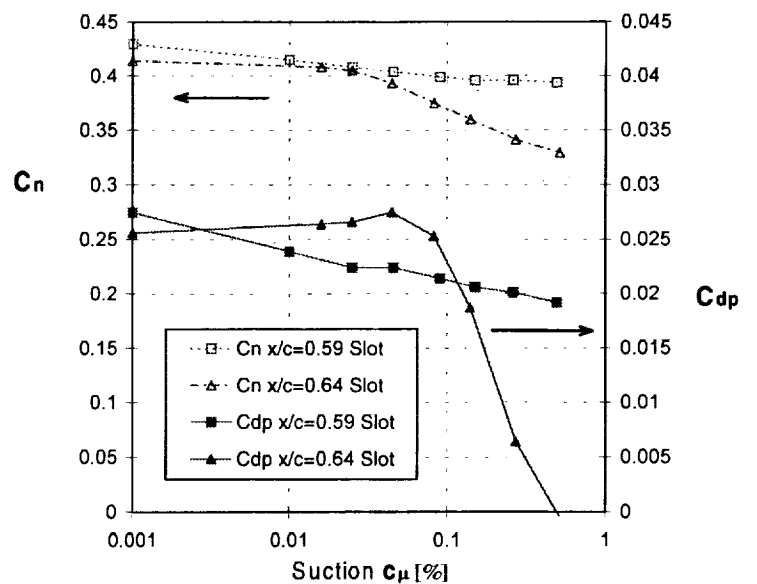
Fig. 27 The effect of the slot location on the integral parameters using suction for control, M=0.25, R_c= 21x10[6.]
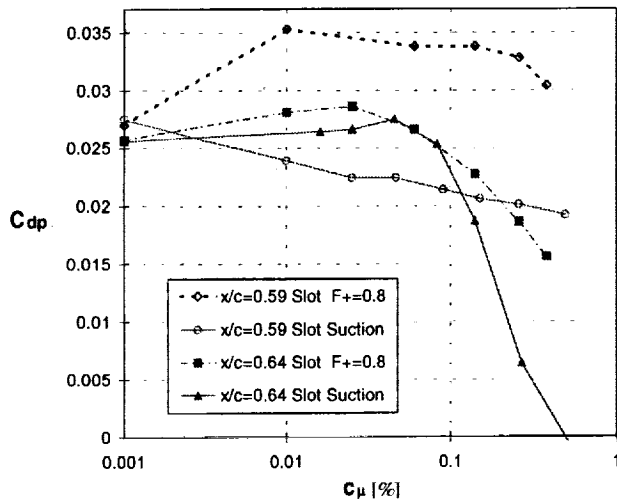
Fig. 28 The effect of the slot location on form-drag reduction using steady suction and periodic excitation for control, M=0.25, R_c= 21x10⁶
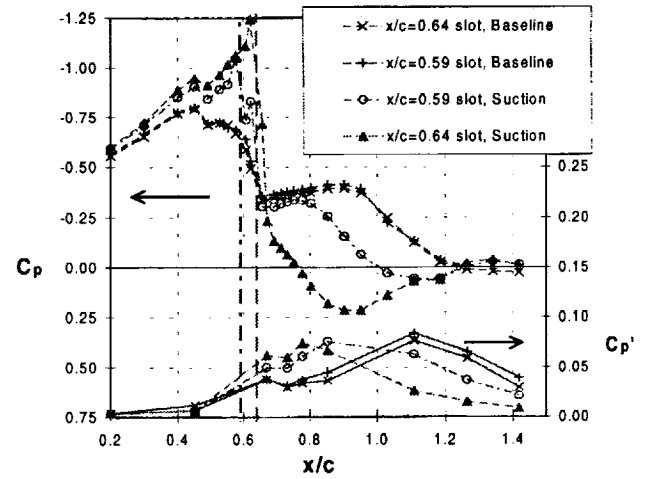
Fig. 30 The effect of the slot location on Cp & Cp' using steady suction with cμ=-0.5% for control, M=0.25, R_c= 21x10⁶.

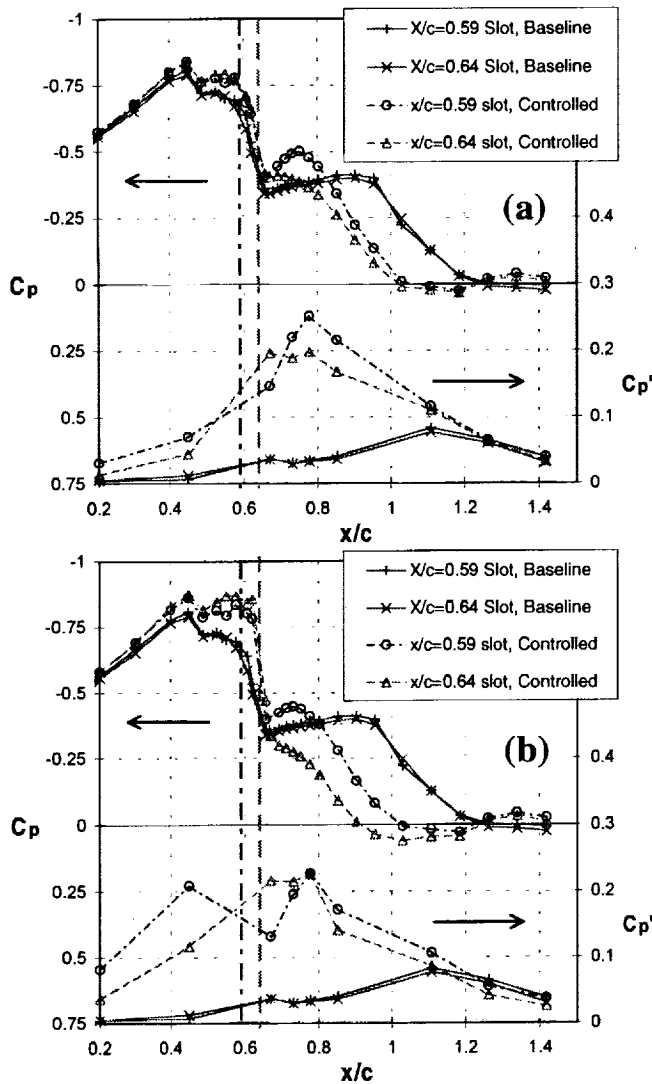**Fig. 31** Slot location effect on baseline Cp & Cp',M=0.65, R_c= 29x10

Fig. 29 The effect of the slot location on Cp and Cp' using F⁺=0.8 for control, M=0.25, R_c= 21x10⁶: (a) <cμ>=0.06% and (b) <cμ>=0.38%.
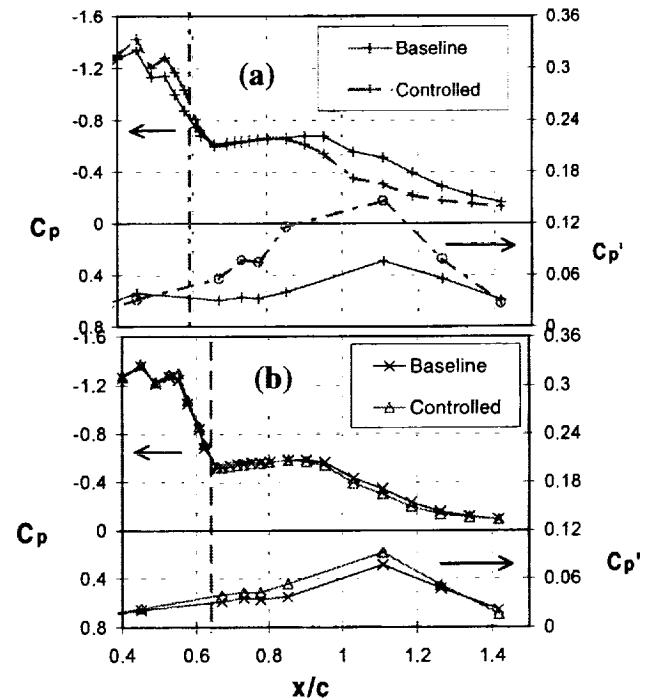
Fig. 32 The effect of F⁺=0.62 and <cμ>=0.03% on Cp & Cp', M=0.6⁵ R_c= 29x10⁶: (a) x/c=0.59 slot, (b) x/c=0.64 slot.